THE ASTROPHYSICAL JOURNAL, 410:686–695, 1993 June 20

THREE-DIMENSIONAL SIMULATIONS OF PROTOSTELLAR JETS

ELISABETE M. DE GOUVEIA DAL PINO
Harvard-Smithsonian Center for Astrophysics and University of São Paulo, Instituto Astronomico e Geofisico, Av. Miguel Stefano, 2400, São Paulo, 04301-904, Brazil

AND

WILLY BENZ
University of Arizona, Steward Observatory and Lunar and Planetary Laboratory, Tucson, AZ 85721
Received 1992 September 21; accepted 1992 December 11

ABSTRACT

We present the first results of fully three-dimensional (3D) simulations of supersonic, radiatively cooling jets using the smoothed particle hydrodynamics technique (SPH). Our results qualitatively agree with the two-dimensional (2D) simulations of Blondin, Fryxell, & Konigl (1990), although the removal of the axisymmetry has resulted in relevant structural differences, especially at the jet head where a cold shell is formed from the condensation of shock-heated material. In particular, we found that the shell is not only dynamically unstable but also may undergo oscillations in density, which are attributed to global thermal instabilities. These effects may have important consequences on the dynamics and emission pattern of the observed HH objects associated to young stellar jets. We discuss the implications of our results in the interpretation of the observed properties of the stellar jets and HH objects. We also compare the structure of radiative cooling and adiabatic 3D jets.

Subject headings: galaxies: jets — hydrodynamics — ISM: jets and outflows — shock waves — stars: mass loss — stars: pre–main-sequence

1. INTRODUCTION

Many young stellar objects (YSOs) eject highly collimated supersonic jets (see Mundt, Brugel, & Buhrke 1987, hereafter MBB, for a review of their properties). They present projected lengths between 0.01–0.8 pc, and a ratio of length to width up to $\approx 30:1$ (e.g., MBB; Reipurth 1989a). The emission along the jet, mainly due to low-excitation lines (e.g., [S II]), is concentrated in rather regularly spaced knots. Assuming that the line emission is produced by shock-heated gas within the flow, one estimates mean jet densities $n_j \approx 20$–100 cm^{-3} (MBB). The observed line-ratios of the emitting matter in the knots imply shock velocities of the order of 40–100 km s^{-1}. The deduced jet propagation velocities are given by $v_j \approx 100$–400 km s^{-1} which correspond to Mach numbers $M_j \approx 10$–40 for an assumed jet temperature of 10^4 K. Many of these jets are apparently denser than the ambient gas. Observations of the HH 1, HH 2, HH 39, HH 47A, HH 47C regions indicate a jet to ambient density ratio of ≈ 1–2 (MBB), while observations of the HH 34 region suggest a density ratio 10 (e.g., Morse et al. 1992).

There is a correlation between these supersonic jets and the Herbig-Haro (HH) objects which are shocked line-emission features exhibiting proper motions of 50–200 km s^{-1}. In some cases (e.g., HH 1, HH 34, and HH 47) (MBB; Hartigan, Raymond, & Meaburn 1990; Morse et al. 1992), a collimated beam terminates in a HH object which resembles a bow shock at the head of the jet. In other cases (e.g., HH 7–HH 11, HH 34, HH 111) (Reipurth 1989a, b), the HH objects appear to be emission regions inside the outflow, i.e., knots in the jet. In general, HH objects with evidence of a bow shock structure are internally highly structured, i.e., they are rather knotty (e.g., HH 1, HH 2, HH 19, and HH 12) (Bohm & Solf 1985; Strom, Strom, & Stocke 1983; Mundt et al. 1984). Also, structural and brightness variability have been detected in HH 1 and HH 2 (Herbig & Jones 1981; Brugel et al. 1985).

Previous, one-dimensional, stationary, radiative bow shock models around a "bullet" or rigid obstacle (e.g., Raga & Bohm 1985, 1986, 1987; Hartigan, Raymond, & Hartmann 1987) have successfully predicted some of the observational properties of the HH objects. However, with the increasing evidence of correlation of the HH objects with supersonic YSO jets, it became clear that the approximation of a rigid obstacle instead of a gaseous jet, for the formation of the bow shock was inadequate to explore the overall range of properties of the HH objects.

Supersonic flows occurring on extragalactic scales, have been the focus of much theoretical work over the last decade. Extensive numerical hydrodynamical simulations have been performed for *adiabatic* jets (e.g., Norman 1990 and references therein) in order to study their structure, stability properties, and propagation through the ambient medium. Considering, however, the typical number densities and shock velocities of the YSO jets and HH objects given above, the cooling time of the shock-heated material (of the order or less than 100 yr) is in general smaller than the evolutionary time of these objects (for example, the inferred age of the HH 34 jets is ≈ 1000 yr) and the assumption of an adiabatic gas is therefore inappropriate for YSO jets.

Recently, Raga (1988), Tenorio-Tagle, Cantò, & Rozyczka (1988, hereafter TCR), and Blondin, Fryxell, & Königl (1990, hereafter BFK), concerned with the dynamics of YSO jets and HH objects, have performed numerical simulations of two-dimensional, axisymmetric, supersonic jets including the effects of radiative cooling, neglected in the previous analysis. The first two works have mainly concentrated on the jet head (Raga 1988) and on the initial shock collimation of an overpressured conical beam (TCR), whereas BFK have simulated the entire evolution of axisymmetric beams. They found that the structure of cooling jets is similar to that of adiabatic jets but with relevant distinctions. In particular, they verified that (1) a cold, dense shell condenses out of the shocked gas at the head of the jet. The shell is dynamically unstable and eventually fragments

into clumps; (2) the beam is less collimated and has weaker and fewer internal shocks than its adiabatic counterparts; and (3) for high cooling rates, the condensed material collects at the head of the jet forming an extended plug of cold gas. BFK suspect, however, that this accumulation of material at the jet axis is due to the imposed axisymmetry and is associated with numerical inaccuracies at the coordinate singularity at the axis ($r = 0$), where they have assumed reflecting boundary conditions.

The comparison of the 2D simulations with the observations is limited by the assumed axisymmetry. 3D simulations are then desirable: (1) to clarify the extent to which the axisymmetric features occur; (2) to explore a more realistic picture of the developing features, particularly, at the head of the jet, and its association with the observed YSO jets and HH objects; and (3) to check the development of nonaxisymmetric instabilities which are prohibited in 2D simulations and can significantly alter the axisymmetric flow structures (e.g., Norman 1990).

In this work, we present the first results of fully 3D simulations of radiative cooling jets. The simulations are performed with a modified version of the 3D Cartesian Smoothed Particle Hydrodynamics (SPH) code described by Benz (1990, 1991). We examine in detail the role of the dynamical (Kelvin-Helmholtz & Rayleigh-Taylor) and the thermal instabilities in the structure and evolution of radiative cooling jets and qualitatively compare our models with the stellar jets and HH objects. The main differences between 3D adiabatic and cooling jets are also examined, and our results are compared with the previous 2D simulations of cooling jets. A summary of our main results has been presented in Gouveia Dal Pino & Benz (1993a, 1993b).

In § 2 we discuss briefly the basic theoretical properties of adiabatic and nonadiabatic jets. In § 3 we describe the assumptions of our numerical model and the assumed initial and boundary conditions. In § 4, we present the results of our hydrodynamical simulations, and in § 5 we summarize our results and discuss their application to the observed YSO jets and HH objects.

2. THEORETICAL GROUNDS

The basic theoretical properties of adiabatic and cooling jets are summarized by Norman (1990) and BFK, respectively. A supersonic jet propagating into a stationary ambient gas will develop a shock pattern at its head which also denominated working surface. The beam outflow is decelerated in a *jet shock* or *Mach disk*. The impacted ambient material is accelerated by a forward *bow shock* (e.g., Blandford & Rees 1974).

The velocity of advance of the bow shock can be estimated by balancing the momentum flux of the jet material at the jet head with the momentum flux generated by the ambient medium at the bow shock:

$$[\rho_j(v_j - v_{\rm bs})^2 + p_j]R_j^2 \approx (\rho_a v_{\rm bs}^2 + p_a)R_h^2 , \quad (1)$$

where v_j is the jet velocity, $v_{\rm bs}$ is the velocity of advance of the bow shock, ρ_j and ρ_a are the mass densities of the jet and ambient material, respectively, and p_j and p_a are the thermal pressures in the jet and ambient medium, respectively, which can be neglected in equation (1) for highly supersonic flows. R_j is the radius of the jet beam and R_h is the radius at the jet head. The bow shock velocity is then roughly given by

$$v_{\rm bs} \approx v_j[1 + (\eta\alpha)^{-1/2}]^{-1} \quad (2)$$

where $\eta = n_j/n_a$ is the ratio of the jet number density to the ambient number density, and $\alpha = (R_j/R_h)^2$. We found that this approximate relation is verified in our simulations (see § 4). Initially, the radius $R_h \approx R_j$ but it can change with time and cause some variation of the propagation velocity $v_{\rm bs}$ (e.g., Cioffi & Blondin 1992).

From equation (2) we see that for a low-density jet ($\eta \ll 1$), $v_{\rm bs} \ll v_j$ and the jet material is constantly decelerated at the end of the jet (at the jet shock). The high-pressure, shocked gas drives a flow back along the jet forming a cocoon of shock-heated waste material. A dense jet, on the other hand, for which $v_{\rm bs} \approx v_j$, will simply plow through the ambient medium at close to the jet velocity without accumulating much waste of gas in the cocoon. The ambient material that traverses the bow shock will form a shroud of ambient shock-heated gas surrounding the beam/cocoon structure.

Initially, a cooling jet behaves approximately adiabatically. But, after a time $t_{\rm cool}$, the jet develops a shell of dense gas formed by the cooling of the shock-heated gas in the working surface, where

$$t_{\rm cool} \approx \frac{(n_e + n_{\rm H})kT_s}{(\gamma - 1)n_e n_{\rm H}\Lambda(T_s)} \quad (3)$$

is the cooling time of the gas immediately behind the shock, $n_e n_{\rm H}\Lambda(T_s)$ is the cooling rate in units of energy per unit volume and time, n_e and $n_{\rm H}$ are the postshock electronic and hydrogen number density, respectively (which for a strong shock are $\approx 4n_{e,0}$ and $4n_{{\rm H},0}$, respectively, where $n_{e,0}$ is the preshock electronic number density and $n_{{\rm H},0}$ is the preshock hydrogen number density), γ is the ratio of specific heats of the gas, k is the Boltzmann constant, and T_s is the immediate postshock temperature

$$T_s = \frac{2(\gamma - 1)\mu v_s^2}{(\gamma + 1)^2 k} , \quad (4)$$

where v_s is the shock speed and μ is the average mass per particle.

The importance of the cooling can be quantified in terms of the cooling length, $d_{\rm cool}$, for the gas to cool to some low value ($\approx 10^4$ K) behind one of the shocks. Cooling length $d_{\rm cool}$ is approximately given by

$$d_{\rm cool} \approx \frac{v_s t_{\rm cool}}{4} \quad (5)$$

(where $v_s/4$ is the postshock speed for a strong shock).

Thus, defining the cooling parameter $q_s = d_{\rm cool}/R_j$, one expects that if $q_s \gg 1$, the shock-heated gas does not have time to cool before leaving the working surface and can be considered adiabatic. If, on the other hand, $q_s < 1$, the shock is fully radiative and the postshock gas loses the bulk of its internal energy in a relatively short distance. In this case, the jet develops a shell of dense gas formed by the cooling of the shock-heated gas in the working surface.

Considering the radiative cooling function $\Lambda(T)$ (due to collisional excitation and recombination) for a cosmic abundant gas, one can evaluate q_s numerically for a one-dimensional steady state shock (see Hartigan, Raymond, & Hartmann 1987). Using the cooling function of Kafatos (1973), BFK evaluated q_s for a gas cooling from $T \approx 10^6$ to 8000 K:

$$q_s \approx 4 \times 10^{16} n_0^{-1} R_j^{-1} v_{s,7}^4 \quad (6)$$

for $v_{s,7} \geq 0.9$, where $v_{s,7}$ is the shock velocity in units of 10^7 cm s^{-1}, and n_0 is the preshock number density of nuclei. This relation for $d_{\rm cool}$ is in rough agreement with that evaluated by Hartigan et al. (1987), but it is a few times larger than that determined by time-dependent cooling calculations (e.g., Innes, Giddings, & Falle 1987) which take into account the history-dependent effects of nonequilibrium ionization and nonlocal radiative transfer in the evaluation of $\Lambda(T)$.

Using equations (2) and (6), the cooling parameter for the bow shock is

$$q_{\rm bs} \approx 4 \times 10^{16} n_{a,0}^{-1} R_j^{-1} v_{j,7}^4 [1 + (\eta\alpha)^{-1/2}]^{-4} \quad (7)$$

where $n_{a,0}$ is the ambient number density of nuclei (note, for example, that for a completely ionized gas of primordial abundances $n_{a,0} \approx n_a/2$).

And noting that the jet shock velocity is given by $v_{js} \approx v_j - v_{\rm bs}$, the cooling parameter for the jet shock is

$$q_{\rm js} \approx q_{\rm bs} \eta^{-3} \alpha^{-2} \quad (8)$$

Assuming $\alpha \approx 1$, these relations imply that a heavy jet ($\eta \gg 1$) will exhibit much stronger cooling behind the jet shock and most of the gas that accumulates in the shell in this case consists of shocked jet material. The reverse situation holds for light ($\eta \ll 1$) jets. It is relevant to notice that, according to equation (6), equation (8) is valid only if the jet shock velocity $v_{\rm js,7} \geq 0.9$. In fact, for $v_{\rm js,7} < 0.9$, the cooling length parameter in equation (6) tends to increase with decreasing shock velocity (e.g., Raga & Binette 1991). As a consequence, $q_{\rm js}$ in equation (8) will increase with η, so that in this case, for jets with large enough η, the jet shock will be essentially adiabatic (while the bow shock will be possibly nonadiabatic).

The density of the dense shell ($n_{\rm sh}$) can be estimated by balancing the thermal pressure of the cooled gas to a temperature $T_{\rm min}$ with the ram pressure of the ambient medium

$$n_{\rm sh} \approx \frac{\mu n_a}{k T_{\rm min}} v_j^2 [1 + (\eta\alpha)^{-1/2}]^{-2}, \quad (9)$$

For a gas cooling to $T_{\rm min} \approx 10^4$ K with $v_j \approx 250$ km s^{-1}, $\alpha \approx 1$, and $n_a \approx 20$ cm^{-3}, $n_{\rm sh} \approx 10^3$ cm^{-3}.

3. NUMERICAL TECHNIQUE

3.1. *The Code*

The hydrodynamics conservation equations are solved using the smoothed particle hydrodynamics technique (SPH). We have used a modified version of the 3D Cartesian SPH code, which is described in detail by Benz (1990, 1991). SPH is a gridless, Lagrangian approach to fluid dynamics which avoids the problems associated with mesh distortion and tangling, often found in grid-based codes. Each mass element, or particle, is characterized by its position in the phase space ($\boldsymbol{r}$, $\boldsymbol{v}$), its mass (m), and its specific internal energy (u). The particles track the matter and move with it.

The jet and the ambient gas are treated as a single, completely ionized fluid with a ratio of specific heats $\gamma = 5/3$ and an ideal equation of state $p = u(\gamma - 1)\rho$. With this assumption of complete ionization, the average mass per particle is maintained constant.

The time integration is done using a second order Runge-Kutta-Fehlberg integrator. The shock waves which arise in the flow are treated by the Newmann-Ritchmyer artificial viscosity technique. A piecewise hierarchical tree method is used to find the particle neighbors (Benz et al. 1990).

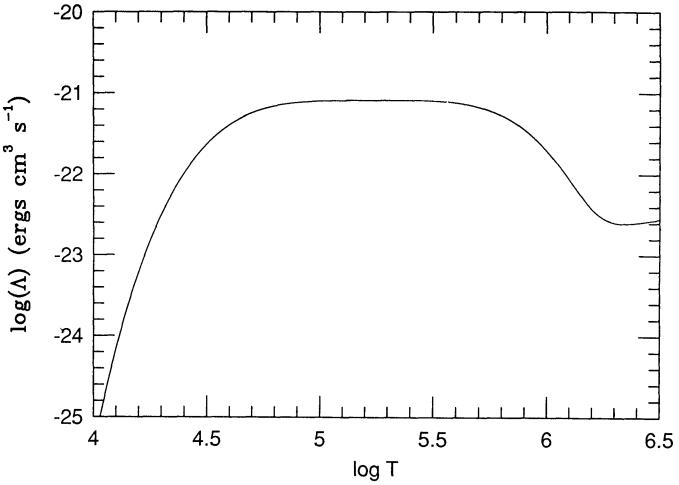

FIG. 1.—The time-independent cooling function used in the numerical simulations. This function is adapted from Katz (1989) and corresponds to a gas of cosmic abundances cooling from 10^6 K.

The radiative cooling (due to collisional excitation and recombination) has been implicitly calculated using the local time-independent cooling function $\Lambda(T)$ calculated by Katz (1989) for a gas of cosmic abundances, cooling from $T = 10^6$ K (see Fig. 1). We suppressed the cooling below $T \approx 10^4$ K, where it becomes highly dependent on the transfer of ionizing radiation and where the assumption of completely ionized flow breaks down.

3.2. *Initial and Boundary Conditions*

We have assumed a uniform ambient gas which is represented by a 3D rectangular box. A collimated, supersonic jet of radius R_j is continuously injected in the bottom of the box which has dimensions of 30 to $38R_j$ in the z-axis direction and $-6R_j \leq x, y \leq 6R_j$ in the transverse directions x and y. In the simulations, two different geometries have been considered in the jet inlet where the jet gets into the ambient box: (1) jets with a square-shaped cross section and (2) jets with initial circular cross-section (see § 4). The boundary conditions on the x and y peripheries of the box are assumed to be periodic, particles being able to cross on one side and re-enter on the other side. The boundary conditions on the z peripheries are continuitive ($\partial \boldsymbol{v} = 0$), particles being removed from the system whenever crossing the $z_{\rm min}$ or $z_{\rm max}$ boundaries (see Herant 1992). The reason for assuming periodic boundaries on the transverse directions x and y is that they provide the smoothest boundaries in a SPH scheme. If the x and y dimensions of the ambient "box" are large enough, the periodic condition will reproduce quite well the physical properties of the ambient medium which is infinite and approximately homogeneous. On the other hand, as the cocoon and the shroud evolve and fill up the ambient "box," weak reflected shock waves may develop close to the x and y boundaries (see discussion below in § 4). However, as long as those shock structures remain close to the outer boundaries and do not propagate inside the cocoon and jet regions, they will have no relevant effects on the physical structures which develop in those regions.

We started the calculations with 67,000 to 85,000 particles. The evolution problem has been parameterized by the dimensionless numbers: (1) $\eta = n_j/n_a$ (the ratio between the input jet density and the ambient density); (2) $M_a = v_j/c_a$ (the ambient Mach number, where c_a is the ambient sound speed); (3) $K_p =$

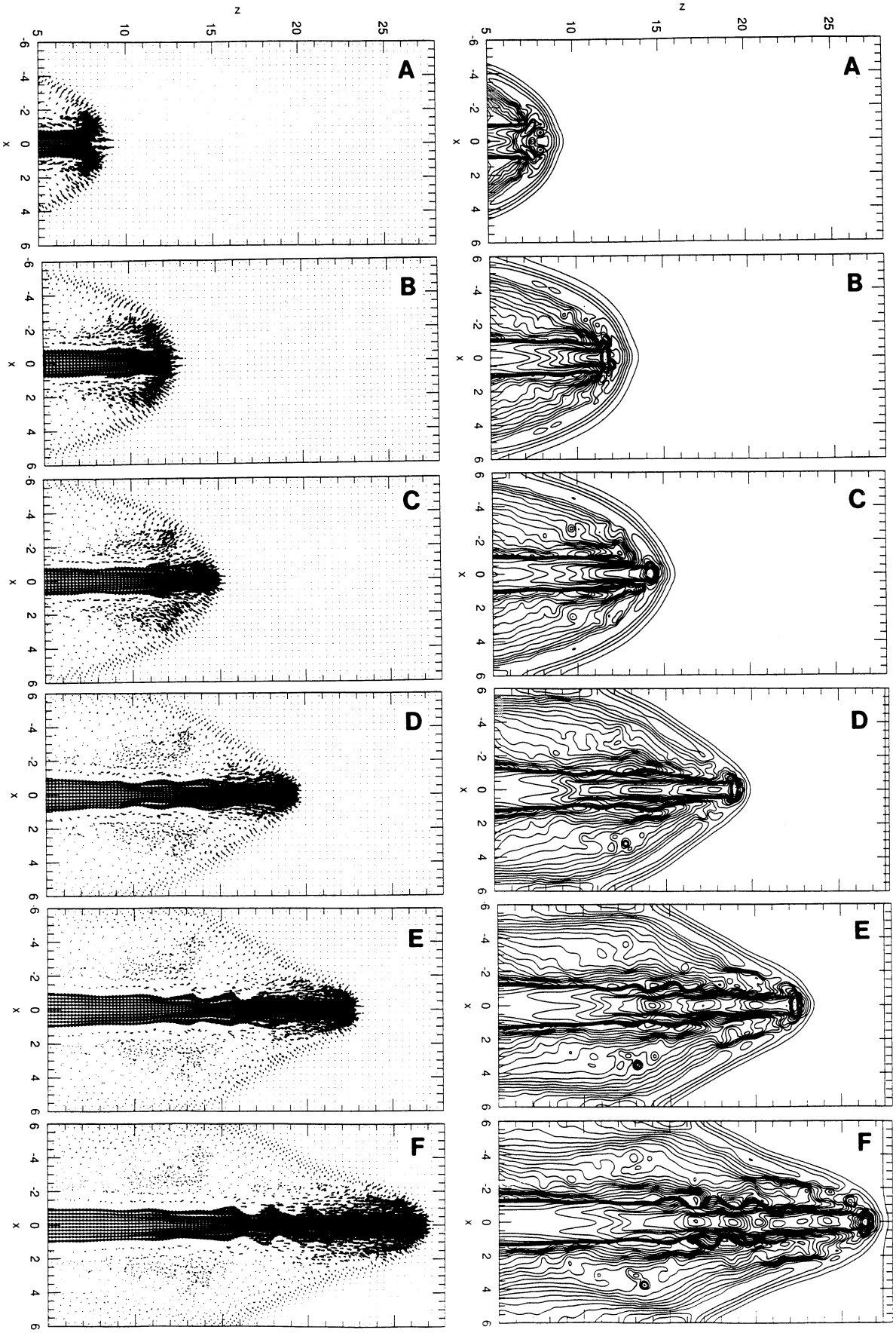

FIG. 2.—The central density contour and the velocity distribution of an adiabatic jet with $\eta = n_j/n_a = 1$, $n_j = 20\ \mathrm{cm}^{-3}$, $R_j = 2 \times 10^{16}$ cm, $v_j = 250\ \mathrm{km\ s}^{-1}$, and $M_j = M_a = 20$. The contour lines of the gas density are separated by a factor of 1.2 and the density scale covers the range from ≈ 0 up to $\approx 302\ \mathrm{cm}^{-3}$. The z, and x coordinates are in units of R_j. The entire evolution in these plots corresponds to a jet age $t = z/v_{\mathrm{bs}} \approx 1115$ yr. The times shown are (*a*) 380 yr; (*b*) 570 yr; (*c*) 670 yr; (*d*) 835 yr; (*e*) 960 yr; and (*f*) 1115 yr.

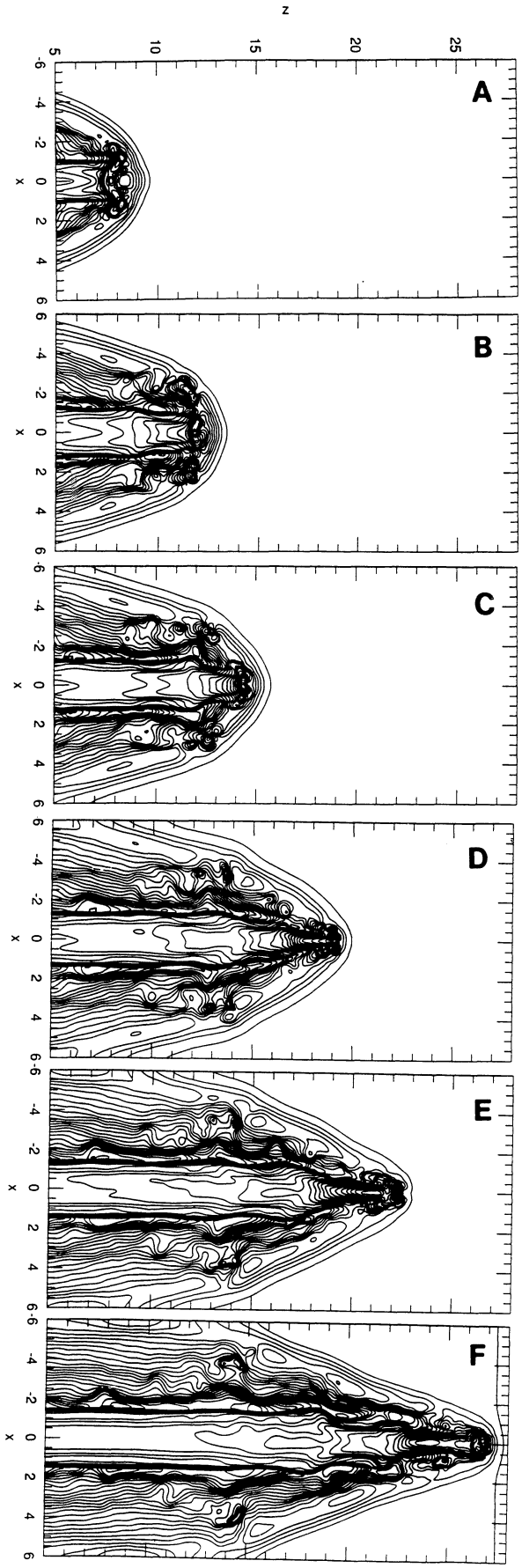

p_j/p_a (the input pressure ratio) which has been assumed to be initially equal 1 in all simulations; and (4) q_{bs} (which is given by eq. [7]).

4. HYDRODYNAMICAL SIMULATIONS

Figures 2 and 3 show the central density contours of an adiabatic (Fig. 2) and a cooling (Fig. 3) jet. The velocity distribution of the adiabatic jet is also shown. Both figures have the same initial parameters of the standard model of BFK, i.e., a density ratio $\eta = n_j/n_a = 1$, a jet density $n_j = 20$ cm^{-3}, a jet radius $R_j = 2 \times 10^{16}$ cm, a jet velocity $v_j = 250$ km s^{-1}, and jet and ambient Mach numbers $M_j = M_a = 20$, corresponding to an initial jet gas temperature $T_j = 6704$ K. The initial cooling length parameters in Figure 3 are given by $q_{bs} = q_{js} \approx 0.63$. The differences in the q_s parameter in the present analysis relative to BFK are due to differences in the assumed atomic constants (we have assumed a gas with a mean molecular weight per particle equal to 0.59, and a hydrogen relative mass abundance equal to 0.75). The entire evolution in these plots corresponds to a jet age $t = z/v_{bs} \approx 1115$ yr. In our simulations, we found that the velocity of propagation of the bow shock tends, in general, to increase with time. This acceleration is directly related to the decrease of the radius of the head of the working surface, R_h, with time (see eq. [2]). In Figures 2 and 3, the bow shock velocity is initially $v_{bs} \approx 125$ km s^{-1}, which is in agreement with equation (2) for $\alpha = 1$. At the end of the integration (Figs. 2*f* and 3*f*), v_{bs} has increased to ≈ 153 km s^{-1} and $\alpha \approx 2.5$; again equation (2) is approximately verified. This increase in v_{bs} corresponds to an acceleration rate of the order 10^{-9} km s^{-2}.

In Figure 3, a dense shell develops in the cooling jet, in agreement with BFK. It is formed by the cooling of the shock-heated gas in the working surface. This gas corresponds to the waste of gas that in the adiabatic jet (Fig. 2) is injected into the cocoon and the shroud surrounding the beam. The density in the shell varies from ≈ 286 cm^{-3} (in Fig. 3*a*) to ≈ 1010 cm^{-3} (in Fig. 3*b*), and ≈ 1164 cm^{-3} (in Fig. 3*c*); reaches a maximum ≈ 4100 cm^{-3} (in Fig. 3*d*), and then fades again to ≈ 2420 cm^{-3} (in Fig. 3*e*), and ≈ 890 cm^{-3} (in Fig. 3*f*). (These values are in rough agreement with eq. [9]). This variable behavior of the density of the shell is consistent with the observed variations in brightness observed in some HH objects at the heads of stellar jets (e.g., HH 1 and HH 2, e.g., Herbig & Jones 1981).

The width and the pressure of the cocoon/shroud of the cooling jet (Fig. 3) are smaller than in the adiabatic jet (Fig. 2) due to the fact that, in the cooling jet, much of the internal energy is lost in the radiative shock. The adiabatic jet (Fig. 2), which has a higher pressure cocoon, becomes Kelvin-Helmholtz unstable with the appearance of the reflecting pinch (Figs. 2*d*–2*e*) and helical (Fig. 2*f*) modes which collimate the beam and cause some jet twisting and flapping. This is in agreement with previous simulations of 2D slab jets (Hardee & Norman 1989), although the wavelength of the modes obtained here, $\lambda \approx 3R_j$, is somewhat smaller. On the other hand, the lesser pressure of the cocoon on the beam of the cooling jet (Fig. 3), results in lesser pinch collimation, and the helical effect is not apparent.

FIG. 3.—The evolution of a cooling jet with the same initial conditions of the adiabatic jet of Fig. 2. The initial cooling length parameters are given by $q_{bs} = q_{js} \approx 0.63$. The contour lines of the gas density are separated by a factor of 1.2 and the density scale covers the range from ≈ 0 up to ≈ 3400 cm^{-3}. The times shown are (*a*) 400 yr; (*b*) 575 yr; (*c*) 670 yr; (*d*) 835 yr; (*e*) $t \approx 950$ yr; and (*f*) $t \approx 1115$ yr.

The appearance of the large-scale K-H instability in the maps may have been influenced by an assumed small Reynolds number in the calculations, $\mathrm{Re} = vL/\nu$, where v is the flow velocity, L is a typical length scale characterizing the variations of the physical quantities of the flow (as an example, for jets, one may take $L = R_j$ and $v = v_j$), and ν is kinematic viscosity (in $\mathrm{cm}^{-2}\ \mathrm{s}^{-1}$) of the flow. In most astrophysical situations, as in the stellar jets, the fluid viscosity is extremely small implying high Reynolds numbers. For protostellar jets, for example, the expected average values of Re are of the order $\mathrm{Re} \approx 10^4$–10^5. Now, in our code (and for that matter, in all codes) there are two kinds of viscosity (see Benz 1991): (1) a numerical viscosity associated with the discretization of the differential equations; and (2) an artificial viscosity introduced to allow dissipation of the kinetic energy into shocks. This artificial viscosity is built by assuming $\nu_1 = c_1 l |\mathrm{div}\ \boldsymbol{v}|$, where c_1 is an arbitrary constant and l is a length over which the shock will be smoothed. This viscosity ν_1 has the advantage of being large only when $|\mathrm{div}\ \boldsymbol{v}|$ is large, i.e., in shocks. An additional viscosity term is added in order to smooth out the remaining small-scale fluctuations in the flow: $\nu_2 = c_2 c_s h$, where c_s is the sound speed, and h is a measure of the distance between the particles in the numerical simulation. Thus, the Reynolds number of our numerical simulations may be estimated by taking $\nu \approx \nu_2$. Using from our simulations $h \approx 0.2 R_j$, we find $\mathrm{Re} \propto (R_j/h) M_j \approx 40$–$100$, which is very small compared to the expected Re numbers for protostellar jets. However, the main effect of the viscosity ν_2 in the simulations, is to suppress instabilities which develop on scales smaller than the scale fixed by the viscosity. In other words, the large-scale instabilities that we see in the simulations, like the K-H modes, are probably not being affected by this viscosity and must be real structures. Furthermore, tests made with different numbers of particles (i.e., different resolution) and thus, different Re revealed no significant changes on the structure of the large-scale instabilities.

Figures 3*b*–3*d* show that the dense shell at the head of the jet becomes dynamically unstable and disrupts into clumps. This effect was also detected in BFK axisymmetric simulations. However, the removal of the axisymmetry condition in the present 3D simulations has resulted in a more realistic picture of the features developed in the jet head. The disruption of the shell is caused by the combined effect of nonuniform cooling and the Rayleigh-Taylor instability (e.g., BFK). The high pressure in the cocoon at the jet head, drives oblique shocks at the edge of the beam. The increase in density behind these shocks is accompanied by a decrease in the cooling time, and the gas at the edges cools faster than the gas in the center, forming a ring of denser gas. This prevents the flow of the hotter gas on the axis of escaping to the cocoon. The pressure of this trapped, less dense gas then pushes the center of the shell forward and the shell, being accelerated into the less dense surrounding medium, becomes Rayleigh-Taylor unstable and begins to break up (Fig. 3*c*).

Figures 2 and 3 have been produced with a jet of square-shaped cross section at the inlet. Simulations with identical initial conditions but assuming a circular jet cross section, have revealed essentially the same morphological evolution of the cooling jet of the Figure 3. The only relevant difference is that the jet shell becomes first dynamically unstable in the circular jet than in the square-shaped jet by about a half of the sound crossing time R_j/c_a. This is due to the fact that in the process of formation of the cold dense ring mentioned above, in the case of the circular jet, all the particles of the ring are equidistant of the axis and thus cool uniformly, whereas in the square-shaped jet ring, the particles in the corners of the square, are more distant from the axis resulting, in a more nonuniform cooling of the ring. As a consequence, the efficiency of the ring in confining the gas in the axis is reduced in this case thus, causing the central gas to push the shell forward about a half sound crossing time later than in the circular jet case. All the following jet simulations have been performed with jets of circular cross section at the jet inlet.

We notice that in the region between $x \approx 4$–$6R_j$ and $z \approx 13$–$15R_j$ in Figures 2*e* and *f* (see also Figs. 4*c*, and 4*d* between $x \approx 4$–$6R_j$ and $z \approx 10$–$15R_j$), a weak shock structure develops close to the x boundary which has been reflected from the boundary itself. This structure is a consequence of the assumed periodic boundary condition on x and y edges and is not expected to occur in real jets. As we pointed out in § 3, the choice of a periodic boundary on the transverse directions, although artificial, is quite convenient to smooth the ambient boundaries in a SPH code. The appearance of this structure, however, has no relevant effects on the other realistic features which develop inside the jet, the cocoon, and the bow shock.

Figure 4 depicts the evolution of a cooling jet with $\eta = 3$, $n_j = 60\ \mathrm{cm}^{-3}$, $R_j = 2 \times 10^{16}$ cm, $v_j = 400\ \mathrm{km\ s}^{-1}$, initial $v_{\mathrm{bs}} \approx 254\ \mathrm{km\ s}^{-1}$ and $v_{\mathrm{js}} \approx 147\ \mathrm{km\ s}^{-1}$, $M_a = 11.55$, $M_j = 20$, and initial $T_j = 1.7 \times 10^4$ K. In this case, $q_{\mathrm{js}} \approx 0.39$ and $q_{\mathrm{bs}} \approx 10.5$, implying that a radiative jet ($q_{\mathrm{js}} < 1$) is propagating into an adiabatic ambient medium ($q_{\mathrm{bs}} \gg 1$) and the gas that accumulates in the dense shell consists essentially of shocked-jet material. The entire evolution corresponds to an age $t \approx 780$ yr and the final $v_{\mathrm{bs}} \approx 292\ \mathrm{km\ s}^{-1}$. This small increase in the bow shock propagation velocity is also in agreement with equation (2) and corresponds to an acceleration rate of $\sim 2 \times 10^{-9}\ \mathrm{km\ s}^{-2}$.

The evolution in Figure 4 is similar to that of the jet of Figure 3, but the dense shell is initially thicker and smaller. It also becomes unstable and separates into clumps (Figs. 4*b*–4*d*). The little cooling of the ambient gas, results in a high-pressure shroud which helps to confine the beam and the cocoon. After the disruption, at late times, part of the shell material spills out to the cocoon forming, together with the shell, an elongated plug of cold gas in the head (Figs. 4*c*–4*d*), which resembles the nose cone seen in numerical simulations of strong magnetized jets (see Norman 1990). This effect, also seen in Figures 3*e* and 3*f*, is different from that found in BFK 2D simulations where the extended plug is formed by the accumulation of condensed material along the axis. In BFK case, the accumulation is probably caused by numerical inaccuracies at the jet axis associated with the assumed axisymmetry (see BFK).

As the dense shell of Figure 4 becomes dynamically unstable, its density in the axis undergoes the time oscillations shown in Figure 5. At each time, the pressure in the working surface has two peaks. One peak (labeled with p in Fig. 5) corresponds to the (radiative) shocked jet material and is coincident with the density peak. The other peak (labeled with p_{bs} in Figure 5) corresponds to the (adiabatic) shocked ambient gas. The corresponding temperature at the shell, $T \propto p/n$, is also shown in Figure 5. In the time interval depicted in Figure 5, the jet head moved from $z = 14.5R_j$ to $36R_j$. The oscillations of the density (and the pressure p) have a period $P \approx 165$ yr $\approx 2.5 t_{\mathrm{cool}}$, where t_{cool} is the initial cooling time behind the jet shock. [Note also that $P/t_j \approx 10$ (where $t_j = R_j/v_j$) which is comparable to the Rayleigh-Taylor growth time in the shell $t_{\mathrm{RT}}/t_j \approx 2(vj/100\ \mathrm{km\ s}^{-1})$ (e.g., BFK).] The growth time of each

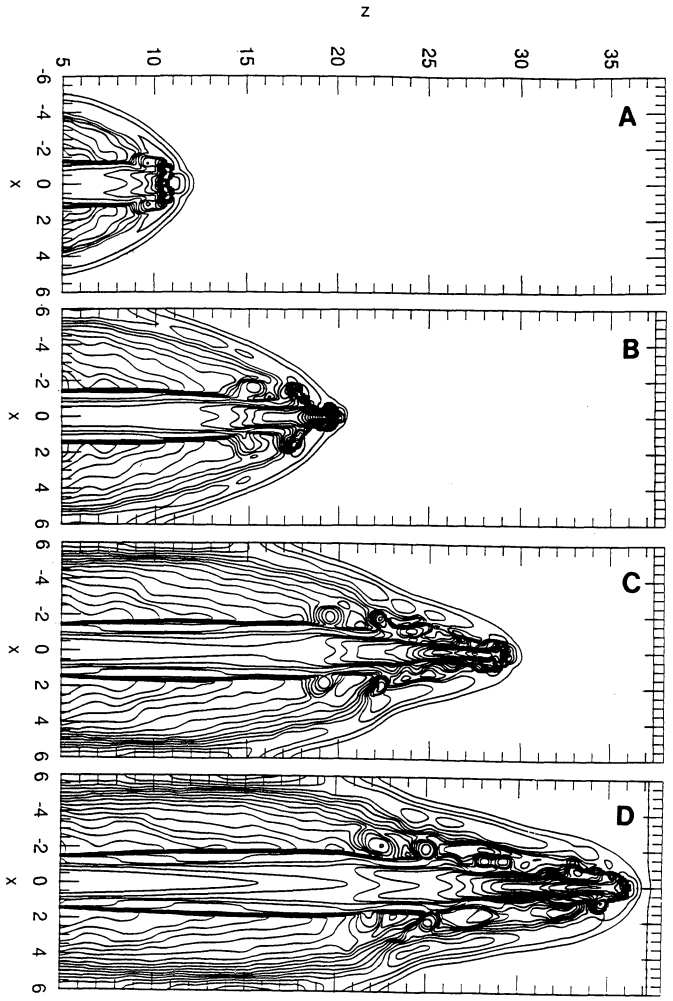

FIG. 4.—The evolution of a cooling jet with $\eta = 3$, $n_j = 60$ cm^{-3}, $R_j = 2 \times 10^{16}$ cm, $v_j = 400$ km s^{-1}, initial $v_{bs} \approx 254$ km s^{-1} and $v_{js} \approx 146$ km s^{-1}, $M_a = 11.55$, $M_j = 20$, initial $q_{js} \approx 0.39$ and $q_{bs} \approx 10.5$. The contour lines of the gas density are separated by a factor of 1.3 and the density scale covers the range from ≈ 0.05 up to $\approx 1400/n_a$. The entire evolution corresponds to an age $t \approx 782$ yr. The time sequence is (*a*) 260 yr; (*b*) 445 yr; (*c*) 640 yr; and (*d*) 782 yr.

density peak is $\approx t_{cool}$ for the first two peaks and $\approx 1.4 t_{cool}$ for the last peak. These growth times are, therefore, of the order of the growth time for thermal instabilities. These results suggest that the working surface is also subject to the development of thermal instabilities. Radiative shocks with velocities higher than ≈ 140 km s^{-1} are known to be susceptible to the *global oscillatory thermal instability* which causes the shock to move back and forth with respect to the shell. This effect has been well studied for one-dimensional radiative shocks (e.g., Bertschinger 1986; Innes et al. 1987; Gaetz, Edgar, & Chevalier 1988, hereafter GEC). It is due to the fact that the cooling length, d_{cool}, behind the shock is strongly dependent on the shock velocity v_s (see eq. [6]). Thus, any small variation in the shock velocity, may cause sudden and relevant variations in d_{cool}, such that a radiative shock, for example, may become suddenly nearly adiabatic by a small increase in the shock velocity. For a radiative shock in which the gas is allowed to cool, the mass flux entering the shock is absorbed in the cold shell and the shock front does not move with respect to the shell. An adiabatic shock, in contrast, must move outward from the shell with $\approx -\frac{1}{3}$ of the incident gas velocity. This is a consequence of the shock jump conditions and the adiabaticity of the postshock flow; the gas can compress to only 4 times the incident gas density, so the shock moves outward to accommodate the additional postshock (adiabatic) gas. The oscillatory pattern in the shell in Figure 5, hence, is produced by variations between a radiative and a nearly adiabatic jet shock phase. If the radiative jet shock is perturbed so that it moves outward from the shell, v_s increases, and so the postshock temperature T_s (eq. [4]), and d_{cool} will greatly exceed the original value. The jet shock becomes nearly adiabatic and continues to move outward (it is the expansion phase). After a postshock cooling time of the nearly adiabatic gas, however, the gas behind the shock has cooled. Therefore, the shock slows down and weakens. The shock velocity then decreases, T_s decreases, and d_{cool} suddenly decreases to a value smaller than the distance shock shell. The jet shock becomes again radiative. It falls with the flow toward the shell and the density in the shell greatly increases as d_{cool} decreases (it is the compressive phase). As the collapsing structure goes in the direction of the shell, the gas is repressurized by collision and drives a nearly adiabatic shock back again. The expansion phase is expected to be longer than the collapsing phase (GEC), as indicated by Figure 5. According to GEC, a radiative shock hitting a wall at 130 km s^{-1} will oscillate for $\approx 5 \times 10^{11} n_0^{-1}$ s before settling down and a shock at 150 km s^{-1} keeps oscillating for even more than $12 \times 10^{11} n_0^{-1}$ s, where n_0 is the preshock density. These time scales are similar to the lifetimes of the jets and much larger than their dynamical time scales t_j. On the other hand, the escape of hot postshock gas to the sides of the jet (in the nearly adiabatic phase), must eventually damp the oscillations as indicated by Figure 5. The density peak which reaches a maximum at $t \approx 412$ yr decreases by a factor ≈ 0.75 after $\Delta t \approx 165$ yr $\approx 2.5 t_{cool}$ and by a factor ≈ 0.55 after $\Delta t \approx 325$ yr $\approx 5 t_{cool}$. Further contribution to the damping of the oscillations may be attributed to the secular increase of v_{bs} (which is related to the decrease of R_h in eq. [2]). This causes, in turn, the decrease of the velocity of the radiative jet shock, $v_{js} \approx v_j - v_{bs}$, which eventually becomes smaller than the threshold value.

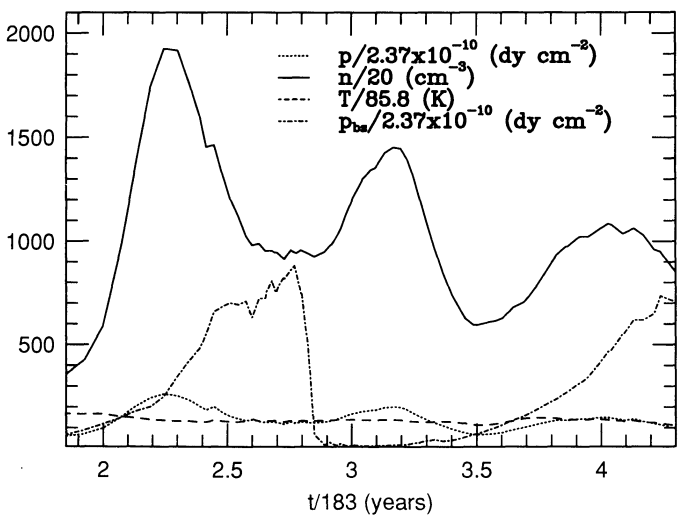

FIG. 5.—The density (n), pressure (p), and temperature (T) of the shell in the axis of the jet of Fig. 4. The time is in units of $R_j/c_a = 183$ yr. In the time interval depicted in the figure, the jet head has moved from $z \approx 14.5 R_j$ to $36 R_j$. The pressure of the shocked ambient gas (p_{bs}) is also shown.

In Figure 5, the pressure of the shocked ambient medium, p_{bs}, also oscillates, but with a different period, $P_{bs} \approx R_j/c_a = 183$ yr. The increasing ram pressure of the shocked jet material in the nearly adiabatic phase ($\approx \rho_j v_{js}^2$) causes the increase of the thermal pressure in the ambient bow shock (see the p_{bs} pressure peak at $t \approx 2.7/183$ yr). After half a period ($\approx 0.5 R_j/c_a$), the p_{bs} pressure has driven the ambient material to the sides into the shroud and p_{bs} then becomes a minimum for another about half a period.

The density oscillations are not apparent in the 2D BFK simulations, probably due to their smaller assumed jet and shock velocities and also, possibly, to the anomalous deposition of condensed material in the axis, mentioned above, in their simulations.

The results above show that the working surface of the radiative jets is not only dynamically but also thermally unstable. Given that the structure of the working surface is continually changing with time, we cannot expect radiative shocks in stellar jets to be steady. In fact, the clump structure of the dense shell with variable density found in the simulations above resembles the knotty and variable structure, with variable emission pattern, observed in some HH objects (e.g., HH 1 and HH 2) (Herbig & Jones 1981; Brugel et al. 1985). This similarity suggests that the variable structure of these HH objects is a consequence of the thermal and dynamical instabilities in the dense shells at the heads of the associated jets.

Figure 6 shows the density contour evolution of a high-density jet with $n_j = 4 \times 10^4$ cm^{-3}, $\eta = 10$, $v_j = 400$ km s^{-1}, $R_j = 10^{15}$ cm, $M_j = 8.28$, and $M_a = 2.62$. Estimated mass flux rates $M_j \approx \pi R_j^2 n_j v_j \approx 5 \times 10^{-2}$–$2 \times 10^{-8}$ $M_\odot$ yr^{-1} for the YSO jets (MBB), may imply jet densities $n_j \geq 10^4$ cm^{-3} in the inner regions of the jet close to the source, for $v_j \approx 400$ km s^{-1} and $R_j \approx 10^{15}$ cm. Figure 6 could thus represent the evolution of YSO jets in the inner regions close to the source. The propagation velocity of the bow shock is initially $v_{bs} \approx 304$ km s^{-1} and increases to $v_{bs} \approx 335$ km s^{-1} at the end of the integration ($t = 12.5 R_j/c_a \approx 26$ yr), while α increases from ≈ 1 to 2.6. This corresponds to a total acceleration rate $\approx 6 \times 10^{-8}$ km s^{-2}.

The initial cooling distance parameters in Figure 6 are $q_{bs} \approx 8.28$ and $q_{js} \approx 2.6 \times 10^{-3}$. As in Figure 3, the shocked ambient material is nearly adiabatic ($q_{bs} > 1$), but the shocked jet material cools much faster ($q_{js} \ll 1$) and the shock is effectively isothermal. The cold shell is thus, very thin and the jet head resembles a "bullet" of dense gas moving ballistically through the ambient medium (see Norman & Silk 1979). The high pressure of the shroud, which is fed by the shock-heated ambient gas, confines the beam/cocoon. Internal shocks, formed via beam pinching, appear in this case. They begin to appear in the beam at a distance $\approx M_j R_j$ and propagate forward with velocities of the order of the advance of the head of the jet ($v_{bs} \approx 304$ km s^{-1}). The mean distance between the internal shocks $\approx 3 R_j$ (or 5 times the local jet radius), is in agreement with the observed jet knots and with the spacing of the reflection mode knots of 2D adiabatic and cooling jet simulations (see Norman, Smarr, & Winkler 1985; BFK; TCR). The maximum density behind these internal shocks is $n_{is}/n_a \approx 500$, while the maximum density in the shell is $n_{sh}/n_a \approx 3300$. Thus, the emission from these shocks must be of lower intensity and excitation than the emission from the head, as required by the observations. Fragmentation of the shell in this case is not apparent as the shell is not well resolved. But, in this case where η is very far from unity, the shell is expected to be susceptible to the (pressure-driven thin shell) Vishniac instability (e.g., Vishniac 1983; Bertschinger 1986) which may eventually cause the fragmentation of the shell.

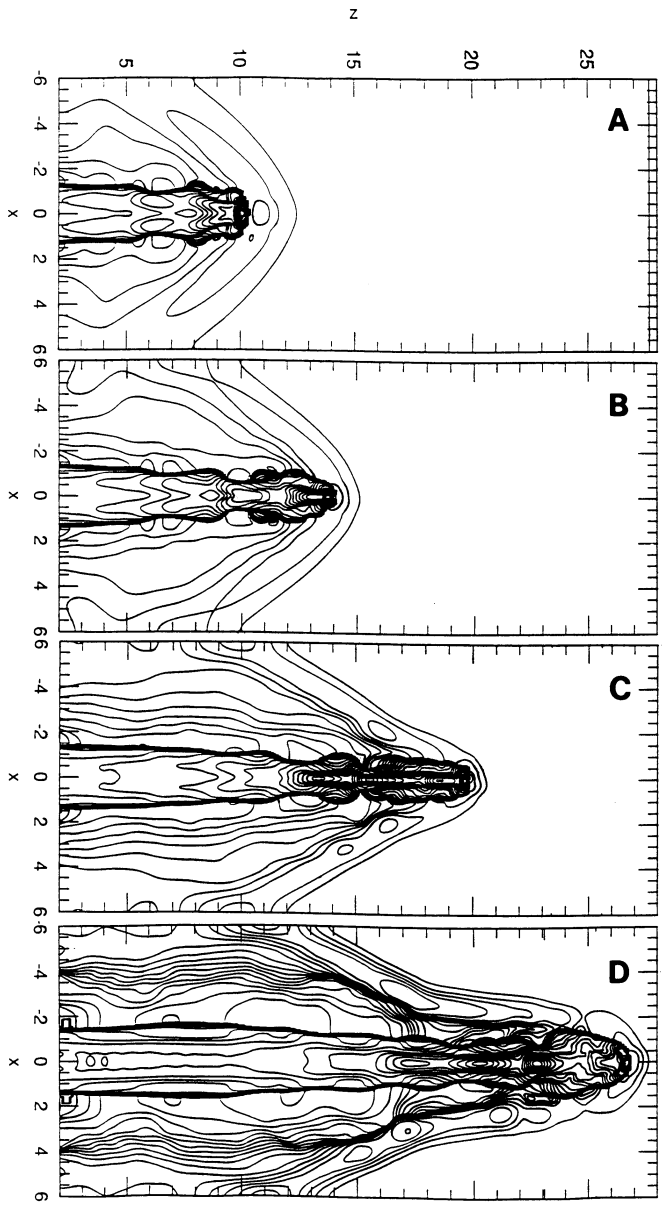

FIG. 6.—The density contour evolution of a high-density jet with $n_j = 4 \times 10^4$ cm^{-3}, $\eta = 10$, $v_j = 400$ km s^{-1}, $R_j = 10^{15}$ cm, $M_j = 8.28$, $M_a = 2.62$, and initial $q_{bs} \approx 8.28$ and $q_{js} \approx 2.6 \times 10^{-3}$. The density contours are separated by a factor 1.3 and the density scales from ≈ 0.01 up to $2900/n_a$. The times shown are (in units of $R_j/c_a = 2.08$ yr): (*a*) 5.1; (*b*) 6.8; (*c*) 9.4; and (*d*) 12.5.

5. CONCLUSIONS AND DISCUSSION

We have presented the first results of fully 3D SPH simulations of radiative cooling jets. They qualitatively agree with the 2D simulations of BFK, although the removal of the axisymmetry has resulted in some relevant structural differences and a more realistic picture of the developing features. Owing to the many simplifying assumptions, particularly in the evaluation of the radiative cooling of the gas, we cannot perform a detailed comparison of our models with the observed stellar jets and HH objects, but we can delineate many of the structural characteristics of these objects.

Our simulations (as BFK's) show the presence of a dense cold shell in the head of the jet formed by the cooling of the shock-heated gas, whenever the cooling length behind the radiative shock, in either the jet or the ambient gas, is $q_s = d_{\rm cool}/R_j \leq 1$. This shell is responsible for most of the emission of the jet.

The shell is, in general, dynamically (Rayleigh-Taylor) unstable and fragments into clumps, which do not present the same symmetric pattern revealed in BFK simulations. The clump shell resembles the knotty structure observed in many HH objects at the bow shock of stellar jets (e.g., HH 1, HH 2, HH 19, HH 12).

The fragmentation of the shell is accompanied by density variations with time. These variations can present an oscillatory pattern if the velocity of the radiative shock is sufficiently high. These oscillations are associated to thermal oscillatory instabilities which cause the radiative shock front to move back and forth with respect to the shell whenever $v_s \geq 140$ km s^{-1} (e.g., GEC). In Figure 4, where the simulation was performed up to $38R_j$ (thus corresponding to a distance large enough for an oscillation pattern to be established if the conditions are appropriate), and where the emission in the head is primarily due to the shocked jet material (since $q_{\rm bs} > 1$ and $q_{\rm js} < 1$), which has a shock velocity $v_{\rm js} \approx 146$ km s^{-1}, density oscillations with a period ≈ 165 yr and peak-density growth times $\approx t_{\rm cool}$ were found in the shell (Fig. 5). This indicates that the shell is subject to the global thermal instability. This effect is not apparent in the BFK simulations, probably due to their smaller assumed jet and shock velocities (see § 4). On the other hand, we found some density variation in the shell even in the case where the shock velocity is below the threshold of ≈ 140 km s^{-1}. This is the case of the jet of Figure 3 where $v_s \approx 125$ km s^{-1}. This result suggests that even in these cases the shock is not steady. The density variations revealed by the simulations may have important effects on the emission pattern of the HH objects and may explain the brightness variability observed in objects like HH 1 and HH 2. In these objects, in particular, optical brightness variations on a time scale ≥ 10 yr (and UV line variability of smaller scales) have been detected (Herbig & Jones 1981; Brugel et al. 1985). Smaller variability periods could be obtained in our model by assuming larger preshock densities and/or smaller shock velocities (but still above the threshold limit ≈ 140 km s^{-1}).

After the disruption, in the late times, part of the clump shell material spills out to the cocoon (Figs. 3 and 4) forming, with the dense shell, an extended plug analogous to the nose cone of magnetically confined jets. This structure is, however, different from the one found in BFK 2D simulations, since in that case, the plug is formed by the coalescence of shell material into a large clump along the axis. This accumulation was probably anomalously caused by numerical inaccuracies in the jet axis of their axisymmetric flow (see BFK). As suggested by Blondin, Königl, & Fryxell (1989), the dispersion of the shell in the late times may be relevant to the interpretation of objects, which exhibit complex velocity and spatial structures like HH 101 (e.g., Hartigan & Graham 1987).

The radiative cooling reduces the thermal pressure which is deposited in the cocoon/shroud. As a result the cocoon/shroud is smaller than in an adiabatic jet and has less pressure to collimate, drive (pinch and helical) Kelvin-Helmholtz instabilities, and reflect internal shocks in the beam (see Figs. 2 and 3). The radiative cooling, therefore, reduces the strength and the number of internal shocks in the jets, a result also verified by BFK, which is consistent with the observed absence of emission from the entire length of some stellar jets. In our simulations, only the very heavy jet ($\eta = 10$) (Fig. 6) showed the formation of internal radiative shocks that are probably due to reflection pinch modes of the Kelvin-Helmholtz instability. The shock spacing of few jet radii is in agreement with the observed knot spacing in stellar jets. A similar knot spacing was found by BFK and in some of the TCR simulations, and is in agreement with the spacing of the reflection mode knots of 2D adiabatic jets (e.g., Norman 1990). The high-density, knotty jet of Fig. 6 could represent a YSO jet in its evolution close to the source.

Our 3D simulations of heavy jets ($\eta > 1$) show a secular increase of the propagation velocity of the bow shock. This acceleration is related to the decrease of the radius at the jet head, R_h, with time and is in agreement with equation (2). In our simulations, we found global acceleration rates $\approx 10^{-9}$–6×10^{-8} km s^{-2}, which increase with the density ratio, η, of the jet system. The reduction of R_h with time also must cause some increase of the cooling length parameter of the bow shock (eq. [7]) and the reduction of the jet cooling length parameter (eq. [8]). The derived values of the variations of the propagation velocities are, however, somehow dependent on the resolution and boundary conditions of the numerical scheme (see also Kossl & Muller 1988). Simulations of adiabatic diffuse jets ($\eta < 1$) show, in contrast, secular decrease in the propagation velocity which is related to the increase of the radius at the jet head with time (Norman, Winkler, & Smarr 1983; Lind et al. 1989).

As in the previous 2D works (Raga 1988; TCR; BFK), in this study we have assumed a history independent, optically thin radiative cooling function. By not following the history-dependent effects of nonequilibrium ionization of the gas or the transfer of ionizing radiation, we may have underestimated the cooling rate in some parts of the postshock region by as much as an order of magnitude (e.g., Innes et al. 1987). However, the conciliation of more accurate ionization and radiative transfer calculations, like those already performed for one-dimensional flows (e.g., Innes et al. 1987), with the present multidimensional hydrodynamical model, would require a substantial amount of computer power. Nonetheless, future work should take into account more detailed ionization and radiative transfer effects although we expect that the gross dynamical features obtained in the present analysis must not change.

We have neglected the effects of the magnetic field. Observations of the HH 34 region (Morse et al. 1992) indicate a magnetic field ≈ 8 μG in front of HH 34 and an energy density in the preshock gas of less than 10^{-3} of the ram pressure, implying that the magnetic field is not relevant in the dynamics of the HH 34, at least in the undisturbed medium. However, the magnetic field may become important once it has been amplified by compression behind a radiative shock. Its presence can, for example, inhibit the maximum density amplification of the cold shell in the cooling jet. BFK estimate that a microgauss field, compressed a hundredfold in the shell is sufficient to begin to stabilize the shell against the Rayleigh-Taylor instability. Gouveia Dal Pino & Opher (1990), in recent study of the development of the thermal condensational instability in YSO jets, have found that the growth of thermal instabilities can be suppressed in the presence of magnetic fields with a magnetic to gas pressure ratio of more than 2. More recently, Innes (1992), investigating the effects of magnetic fields in unstable radiative shocks, verified that a field strength, transverse to the

flow, of 9 mG is sufficient to suppress the global oscillatory instability in a shock with a velocity of 175 km s^{-1}, traveling into a medium with a density of 1 cm^{-3}. In smaller velocity shocks, the oscillations are damped with even smaller field strengths. In the future, it will be fruitful to incorporate magnetic fields in the numerical simulations of radiative cooling jets in order to examine their effects on the structure of the flow, particularly at the shell.

In all the simulations performed in this work, we have assumed a continuous injection of jet material into the ambient medium. Recently, it has been observed that some young stellar jets have a multiple bow shock structure (e.g., Reipurth 1989a) which may, possibly, be due to a noncontinuous injection of the jet material into the ambient medium. Such *recurrent* jets, with noncontinuous but periodic injections, are addressed in other work (Gouveia Dal Pino & Benz 1993b, c, d).

Finally, we would like to address the issue of numerical convergence which is crucial to all computer simulations. We have performed simulations with our 3D Cartesian code which employs the SPH technique. From the results, it is apparent that simulations with 67,000–100,000 particles, are not accurate enough in the cooling regions for one to distinguish between the high-excitation emission region which corresponds to a gas at $T \approx 10^5$ K (where [O III] is formed), and the Balmer and [S II] emission region, which corresponds to $T \approx 10^4$ K. On the other hand, the calculations have captured the salient features of the hydrodynamics, particularly at the head of the jet. The ability of the SPH to realistically simulate the problem with a comparatively low investment of computer work (few days of CPU time in a DEC3110), has its root in the nature of the dynamical and thermal instabilities in the flow. For example, when the dense shell becomes Rayleigh-Taylor unstable, high density, small clumps rise among smaller density, larger regions. For grid codes, the spatial resolution requirement is set by the size of the clumps, which may lead to an over-resolution of the less dense larger regions. Within the SPH approach, the higher density in the clumps automatically implies a higher resolution because of the increased concentration of particles, while the low density regions retain a lower resolution which is satisfactory provided that they are large.

E. M. G. D. P. wishes to acknowledge very fruitful conversations with M. Birkinshaw, A. Dal Pino, Jr., M. Davies, G. Field, M. Herant, J. Navarro, and J. Raymond. We also acknowledge the referee, A. C. Raga whose relevant comments, we believe, have contributed to improve this work. This work was partially supported by the Interamerican Bank of Development and University of São Paulo, and by the Brazilian Agency FAPESP.

REFERENCES

Benz, W. 1990, in Numerical Modeling of Stellar Pulsations: Problems and Prospects, ed. J. R. Buchler (Dordrecht: Kluwer), 269
———. 1991, in Late Stages of Stellar Evolution and Computational Methods in Astrophysical Hydrodynamics, ed. C. de Loore (Berlin: Springer), 259
Benz, W., Bowers, R. L., Cameron, A. G. W., & Press, W. H. 1990, ApJ, 348, 647
Bertschinger, E. 1986, ApJ, 304, 154
Blandford, R. D., & Rees, M. J. 1974, MNRAS, 169, 395
Blondin, J. M., Fryxell, B. A., & Königl, A. 1990, ApJ, 360, 370 (BFK)
Blondin, J. M., Königl, A., & Fryxell, B. A. 1989, ApJ, 337, L37
Bohm, K.-H., & Solf, J. 1985, ApJ, 294, 533
Brugel, E. W., Bohm, K.-H., Shull, J. M., & Bohm-Vitense, E. 1985, ApJ, 292, L75
Cioffi, D. F., & Blondin, J. M. 1992, ApJ, 392, 458
Gaetz, T. J., Edgar, R. J., & Chevalier, R. A. 1988, ApJ, 239, 927 (GEC)
Gouveia Dal Pino, E. M., & Benz, 1993a, in Proc. of STSI Meeting on Astrophysical Jets (Baltimore, 1992 May 12–14), in press
———. 1993b, in Proc. Conf. Subarcsecond Radio Astronomy (Manchester, UK; 1992 July 20–24), in press
———. 1993c, in Proc. 4th Internat. Toki Conf. on Fusion and Astrophysical Plasmas, Toki, Japan, 1992 Nov. 17–20 (in press)
———. 1993d, in preparation
Gouveia Dal Pino, E. M., & Opher, R. 1990, A&A, 231, 571
Hardee, P., & Norman, M. L. 1989, ApJ, 342, 680
Hartigan, P., & Graham, J. A. 1987, AJ, 93, 913
Hartigan, P., Raymond, J. C., & Hartmann, L. 1987, ApJ, 316, 323
Hartigan, P., Raymond, J. C., & Meaburn, J. 1990, ApJ, 362, 624
Herant, M. 1992, Ph.D. thesis, Harvard University
Herbig, G. H., & Jones, B. F. 1981, AJ, 86, 1232
Innes, D. E. 1992, A&A, 256, 660
Innes, D. E., Giddings, J. R., & Falle, S. A. E. G. 1987, MNRAS, 226, 67
Kafatos, M. 1973, ApJ, 182, 433
Katz, J. 1989, Ph.D. thesis, Princeton University
Kossl, D., & Muller, E. 1988, A&A, 206, 204
Lind, K. R., Payne, D. G., Meier, D. L., & Blandford, R. D. 1989, ApJ, 344, 89
Morse, J. A., Hartigan, P., Cecil, G., Raymond, J. C., & Heathcote, S. 1992, ApJ, 399, 231
Mundt, R., Brugel, E. W., & Buhrke, T. 1987, ApJ, 319, 275 (MBB)
Mundt, R., Buhrke, T., Fried, J. W., Neckel, T., Sarcander, M., & Stocke, J. 1984, A&A, 140, 17
Norman, C. A., & Silk, J. 1979, ApJ, 228, 197
Norman, M. L. 1990, Ann. NY Acad. Sci., No. 617, ed. J. R. Buchler & S. T. Gottesman (New York: AIP), 217
Norman, M. L., Smarr, L., & Winkler, K.-H. 1985, in Numerical Astrophysics, ed. J. Centrella, J. LeBlanc, & R. Bowers (Boston: Jones & Bartlett), 88
Norman, M. L., Winkler, K.-H., & Smarr, L. 1983, in Astrophysical Jets, ed. A. Ferrari, & A. G. Pacholczyk (Dordrecht: Reidel), 227
Raga, A. C. 1988, ApJ, 335, 820
Raga, A. C., & Binette, L. 1991, Rev. Mexicana Astron. Af., 22, 265
Raga, A. C., & Bohm, K.-H. 1985, ApJS, 58, 201
———. 1986, ApJ, 308, 829
———. 1987, ApJ, 323, 193
Reipurth, B. 1989a, Nature, 340, 42
———. 1989b, in Proc. ESO Workshop on Low-Mass Star Formation and Pre–Main-Sequence Objects, ed. B. Reipurth (Garching: ESO), 247
Strom, K. M., Strom, S. E., & Stocke, J. 1983, ApJ, 271, L23
Tenorio-Tagle, G., Cantò, J., & Rozyczka, M. 1988, A&A, 202, 256 (TCR)
Vishniac, E. T. 1983, ApJ, 274, 152